JOC The Journal of Organic Chemistry

Article

pubs.acs.org/joc

Degradation of 2,5-Dihydroxy-1,4-benzoquinone by Hydrogen Peroxide under Moderately Alkaline Conditions Resembling Pulp Bleaching: A Combined Kinetic and Computational Study

Takashi Hosoya and Thomas Rosenau*

Department of Chemistry, University of Natural Resources and Life Sciences, Muthgasse 18, A-1190 Vienna, Austria

Supporting Information

ABSTRACT: 2,5-Dihydroxy-1,4-benzoquinone (DHBQ) is one of the key chromophores occurring in all types of aged cellulosics. This study investigates the mechanism of H_2O_2 degradation of DHBQ under conditions relevant to pulp bleaching (3.0% H_2O_2, NaOH, pH 10), to obtain insights useful for improved pulp processing. DHBQ is degraded quantitatively into malonic acid with an activation energy (E_a) of 16.1 kcal/mol and activation entropy ($\Delta^{\ddagger}S^{\circ}$) of ~28 cal/mol·K. Higher concentrations of sodium cations increase the reaction rate. Theoretical computations indicate the formation of an intermediate $\mathbf{I_O}$ having an O−O bridge between C-2 and C-5 of the 1,4-cyclohexadione structure. $\mathbf{I_O}$ undergoes O−O homolysis to form a biradical **Bt**, which is fragmented into malonate anions. The calculated E_a (17.8 kcal/mol) agrees well with the experimental one. Coordination of Na^+ to $\mathbf{I_O}$ and **Bt** decreases their energies and enhances the O−O homolysis rate, which is consistent with the acceleration by sodium cation and the negative $\Delta^{\ddagger}S^{\circ}$. The homolysis of $\mathbf{I_O}$ is much favored over that of the neutral counterpart, with the unpaired electrons of **Bt** being stabilized by the geminal anionic oxygen. This difference in the stability of the intermediates translates into significant variations in the reaction rate and the product distribution between pH 10 and neutral/acidic conditions.

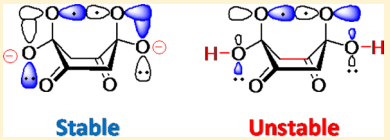

INTRODUCTION

2,5-Dihydroxy-1,4-benzoquinone (DHBQ) has been described as one of the key compounds contributing to discoloration effects of cellulosic materials as a consequence of aging. This overall process is commonly denoted as "yellowing" of the pulp. This comprises natural aging as well as all kinds of stresses by thermal treatment, irradiation, oxidation, or impact by extreme pH conditions. DHBQ is a nearly ubiquitous cellulosic chromophore as it is both a prime survivor of bleaching treatments and a regeneration product from low-molecular weight fragments of cellulose aging.[1] Its exceptional resonance stabilization in alkaline medium is responsible for its resistance toward bleaching chemicals. Most of them, e.g., ozone, hydrogen peroxide, and chlorine dioxide, destroy chromophoric structures mainly by acting on (localized) double bonds. However, the charges, and thus also the double bonds, in the DHBQ-derived dianion are highly delocalized and are thus much more slowly attacked than those in most other quinoid chromophores that lack such resonance stabilization. This makes DHBQ a much better "survivor" of industrial pulp bleaching sequences than other aromatic or quinoid chromophores in pulps.[1] Condensation of carbonyl-containing and carboxyl containing C2−C4 fragments, such as those formed from carbohydrates upon aging, condense under formation of DHBQ as a main product, since it represents a global minimum on the C−H−O thermodynamic formation energy map.

The pulp and paper industries are interested in better, i.e., faster and cheaper, removal of the compound from cellulosic pulps; cellulose scientists search for good methods of DHBQ detection and quantification of its effects on cellulose properties; and conservationists working with historic cellulosic matrices are looking for mild and compatible ways for DHBQ destruction. The chemistry of DHBQ has thus become a point of great interest from several viewpoints in cellulose science. The structure of DHBQ and its resonance-stabilized dianion **CB** is given in Scheme 1.

Scheme 1. Structures of 2,5-Dihydroxy-1,4-benzoquinone (DHBQ) and Its Resonance-Stabilized Dianion CB

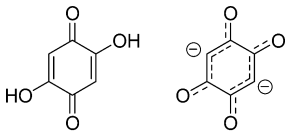

DHBQ **CB**

Several previous accounts have addressed the chemistry of DHBQ, which has recently been reviewed.[2] Its main reaction paths are electrophilic substitution,[3a−h] nucleophilic substitution,[3i] and condensation with amines.[4] However, these works have employed DHBQ as a starting material in organic synthesis or as a target in analytical endeavors. With the "revival" of the compound, which is connected to its pivotal role in cellulose yellowing, the degradation chemistry of DHBQ, i.e., its "discoloration", became a matter of much interest.

We have previously attempted to contribute to the mechanism of H_2O_2 degradation of DHBQ under nonbuffered

Received: July 11, 2013
Published: October 25, 2013

   dx.doi.org/10.1021/jo401486d | J. Org. Chem. 2013, 78, 11194−11203

conditions.[5] Under these conditions, the reaction solution is slightly acidic (pH ≈ 5.5) from the beginning due to the acidity of DHBQ.[2] As shown in Scheme 2, DHBQ is eventually degraded into malonic acid, acetic acid, and carbon dioxide. According to the detailed mechanism, DHBQ forms a primary intermediate $\mathbf{I_{OH}}$ through nucleophilic attack of H_2O_2. Next reaction step, homolysis of the O−O bond of $\mathbf{I_{OH}}$, is rate-determining. β-Fragmentation of the resulting biradical produces oxaloacetic acid **OA** and ketene; see Scheme 2. In this process, the electronic structure remains the most stable singlet (S0) state. **OA** is then further attacked by H_2O_2 and releases carbon dioxide and water to form malonic acid, while ketene is converted into acetic acid by addition of water. This mechanism has been well supported by kinetic analysis, product identification, and computational considerations. However, the conditions in that study were chosen in a way to be as simple as possible and were thus avoiding any additives or adjustment of pH. Although interesting from the scientific point of view, the setting was unfortunately not relevant to cellulose processing, as pulp bleaching with H_2O_2, the so-called bleaching "P-stage", is commonly performed at alkaline pH around 10 and above. Our attempt to verify that the degradation chemistry of DHBQ under such alkaline conditions is similar to that in neutral media failed rather quickly and led us into a different chemistry that, by parallel computational treatment, provided some interesting aspects of DHBQ degradation in particular and bleaching chemistry in general. This is the topic of the present combined experimental and computational study, with which we would like to address the DHBQ degradation under industrially relevant peroxide bleaching conditions, and we hope to provide a solid basis for considerations in cellulose bleaching chemistry and optimization of pulp bleaching sequences.

Scheme 2. Summary of Detailed Reaction Steps of DHBQ Degradation by H_2O_2 under Non-buffered Conditions[5]

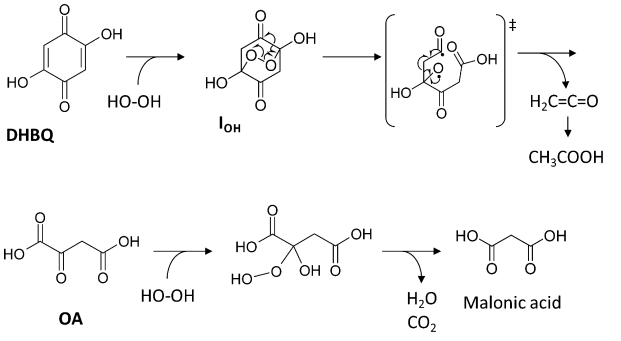

RESULTS AND DISCUSSION

Kinetic Analysis and Product Characterization. In our previous study,[5] we reported that H_2O_2 degradation of DHBQ under nonbuffered conditions was following pseudo-first-order kinetics if an excess amount of H_2O_2 (257 molar equiv of H_2O_2 relative to DHBQ) was used. In the pseudo-first-order approximation, the concentration of DHBQ [DHBQ] at reaction time t is presented by following equation:

$$[\mathrm{DHBQ}] = [\mathrm{DHBQ}]_0\, e^{-kt} \quad (1)$$

where $[\mathrm{DHBQ}]_0$ is the initial concentration of DHBQ and k is the kinetic rate constant. A plot of ln[DHBQ] against t was done to check whether the pseudo-first-order approximation would hold also true under pH 10 degradation conditions. From Figure 1 it is evident that there is a nice, linear relationship between ln[DHBQ] and t, indicating correctness of the pseudo-first-order approximation. The rate constants k at each reaction temperature follow from the slope of the lines. The determined k values ranged from 6.14×10^{-4} to 2.61×10^{-2} s^{-1}, as summarized in Table 1.

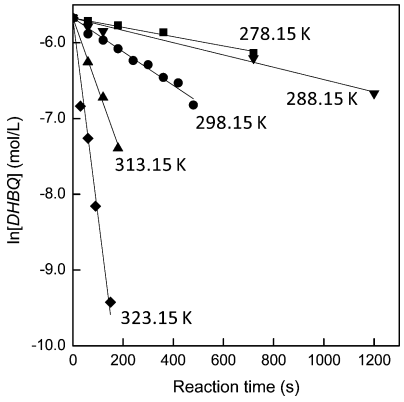

Figure 1. Relationship between ln[DHBQ] and reaction time t at 278.15 K (■), 288.15 K (▼), 298.15 K (●), 313.15 K (▲), and 323.15 K (◆).

Figure 2 shows the corresponding Arrhenius plot of the logarithm of the pseudo-first-order rate constants k (ln k) versus the reciprocal of the reaction temperature (K) to have a linear relationship that allows determination of the activation parameters. The activation energy (E_a) of the degradation was 16.1 kcal/mol, and the activation enthalpy ($\Delta^{\ddagger}H^{\circ}$) was similar at 15.5 kcal/mol; see Table 1. The activation entropies ($\Delta^{\ddagger}S^{\circ}$) were considerably negative (−27.7 to −22.6 cal/mol·K). It is interesting to compare these activation data to those of the reaction under the nonbuffered conditions: under the pH 10 conditions, the activation enthalpies $\Delta^{\ddagger}H^{\circ}$ are lower and the activation entropies $\Delta^{\ddagger}S^{\circ}$ are more negative; see Table 1. In other words, the alkaline degradation is enthalpically favored, but disfavored from the viewpoint of entropy. The $\Delta^{\ddagger}G^{\circ}$ values (21.8−24.1 kcal/mol) are thus moderately smaller for the reaction under the pH 10 conditions, meaning that the reaction proceeds somewhat faster than in neutral medium.

Figure 3A presents the ^{1}H NMR spectrum of the reaction mixture (sample **A**, reaction time 240 s) in DMSO-d_6 obtained at 298.15 K; see the Experimental Section for details of sample preparation. The spectrum shows singlets corresponding to nonreacted DHBQ, its diester with boronic acid, and malonic acid. Here and in the following, all assignments were confirmed by spiking with authentic samples. The boronic ester originated from the borate buffer and was formed under the acidic conditions used to stop the reaction (see also the ^{13}C NMR and ^{11}B NMR spectra of sample **A** in Figure S1 of the Supporting Information for detailed information on the borate ester).[6] Since the signal of malonic acid is overlapping with the water signal in DMSO-d_6, it was thus quantified from the ^{1}H NMR spectrum of sample **B** in D_2O, where the singlet of malonate dianion is neatly separated. Note that sample **B** contains minute traces of acetic acid (see Experimental Section for the difference between samples **A** and **B**). The yields of malonic acid were found to be nearly quantitative (95.4−100%), and thus 2 equiv of malonic acid were formed per

dx.doi.org/10.1021/jo401486d | J. Org. Chem. 2013, 78, 11194−11203

Table 1. Experimental Pseudo-first-order Rate Constants (k) and Activation Parameters in the Degradation of DHBQ by H_2O_2 under pH 10 Conditions

	without sodium sulfate addition[a]				with sodium sulfate addition[d]
		activation parameters[b]			
temp (K)	k (s^{-1})	$\Delta^{\ddagger}H°$ (kcal/mol)	$\Delta^{\ddagger}S°$ (cal/mol·K)	$\Delta^{\ddagger}G°$ (kcal/mol)	k (s^{-1})
278.15	6.14×10^{-4}	15.5	−22.6	21.8	1.60×10^{-3}
288.15	8.20×10^{-4}	15.5	−24.2	22.5	3.70×10^{-3}
298.15	2.22×10^{-3}	15.5	−24.1	22.7	4.10×10^{-3} (3.54×10^{-3})[e]
313.15	1.44×10^{-3} (4.66×10^{-4})[c]	15.5 (19.9)	−27.7 (−16.7)	24.1 (24.9)	2.13×10^{-2}
323.15	2.61×10^{-2} (3.01×10^{-3})[c]	15.5 (19.8)	−23.6 (−14.7)	23.1 (24.5)	2.44×10^{-2}

[a]The reaction solution without sodium sulfate addition also contains some amount of sodium cation since a NaOH-borate buffer is employed. [b]The activation energies (E_a) were determined to be 16.1 kcal/mol under pH 10 conditions and 20.4 kcal/mol under nonbuffered conditions. [c]Values for the nonbuffered conditions from previous study[5] for comparison. Under these conditions, no metal cation is involved in the reaction solution. [d]The concentration of sodium ion is enhanced by the addition of sodium sulfate. The amount of sodium sulfate added was 150 equiv (mole) against DHBQ. [e]Rate constant (k) in the presence of 300 equiv (mole) of sodium chloride.

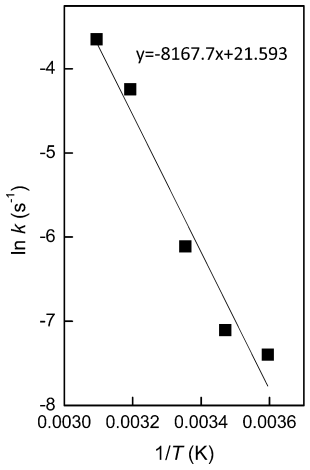

Figure 2. Arrhenius plot of the degradation reaction in the temperature range from 278.15 to 323.15 K.

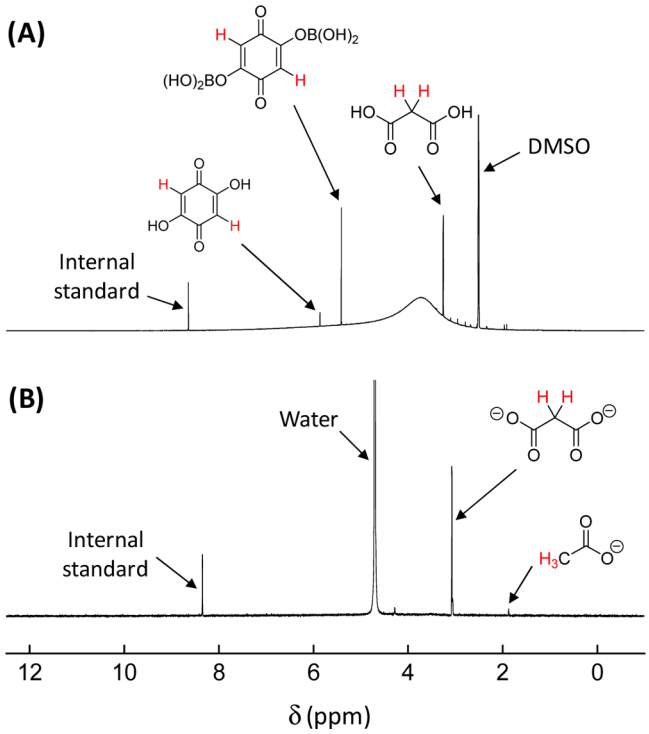

Figure 3. ^{1}H NMR spectra of the degradation reaction at 298.15 K and 240 s, sample **A** in DMSO-d_6 (A) and sample **B** in D_2O (B); see the Experimental Section section for the preparation methods for samples **A** and **B**. In spectrum A, nonreacted DHBQ is found mainly as the diester of boronic acid (from the buffer system, see also Figure S1 in Supporting Information). In the spectrum B, the signal of DHBQ is not detected due to H-D exchange of the protons at C-3 and C-6. The small signal at 4.2 ppm in spectrum B probably correspond to glycolic acid or 2-hydroxymalonic acid, which were detected in GC−MS analysis (see Figure S2 in Supporting Information).

equivalent of degraded DHBQ under the employed pH 10 reaction conditions.[7] Malonic acid was also one of the major products under nonbuffered conditions.[5] However, under those nonbuffered conditions malonic acid, acetic acid and carbon dioxide were formed in equimolar amounts, and only one molecule of malonic acid was produced from one molecule of DHBQ (see Scheme 2). Under pH 10 conditions, by contrast, DHBQ produced almost exclusively malonic acid, and only tiny amounts of acetic acid were seen as byproduct: the ^{1}H NMR spectrum in Figure 3B shows an almost negligible signal of the acetate anion at 1.9 ppm. These results suggested that the degradation mechanism under the moderately alkaline (pH 10) conditions is considerably different from that under the nonbuffered conditions.

The degradation experiment was also carried out in the presence of 150 molar equiv of sodium sulfate (relative to DHBQ). In this case, the concentration of sodium cation is additionally enhanced by the addition of sodium sulfate compared to the original buffer solution. The salt addition significantly increased the reaction rate, as shown in Table 1 (see also Figure S3 in the Supporting Information for the relationship between ln[DHBQ] and t). A similar effect was observed when we substituted sodium sulfate for 300 molar equiv of sodium chloride, maintaining the same amount of the Na^+ relative to DHBQ (Table 1): k was 4.10×10^{-3} s^{-1} in the presence of sodium sulfate and $3.54 \times 10^{-3}s^{-1}$ with sodium chloride, indicating the effect of the cation, but not the anion, to be decisive. This change in the reaction rate by the addition of the salts cannot be explained by changes in the ionic strength of the reaction solution as this would be rather different for the two salts used. It was therefore likely that Na^+ affects some step(s) of the degradation mechanism directly and this way enhances the degradation rate. We will discuss the effect of Na^+ in combination with computational results in the next section. A detailed kinetic analysis of the effect of different alkali, earth alkali, and aluminum salts is the topic of an upcoming report.

dx.doi.org/10.1021/jo401486d | J. Org. Chem. 2013, 78, 11194−11203

Unfortunately, we were unable to determine the activation parameters in the presence of sodium sulfate since the Arrhenius plot was not linear for the most common rate law cases (see Figure S4 in Supporting Information). The reason for this nonlinear relationship is unknown at the moment.

Degradation Mechanism; Quantum Chemical Insights. Quantum chemical calculations were carried out to get some deeper insight into the reaction mechanism. Malonic acid was a major product in the nonbuffered system, formed via intermediate $\mathbf{I}_{OH}$ (see Scheme 2).[5] It appeared reasonable to assume the intermediacy of $\mathbf{I}_O$ under the pH 10 conditions (see Figure 4 and Scheme 3 for the structure), which is the dianionic

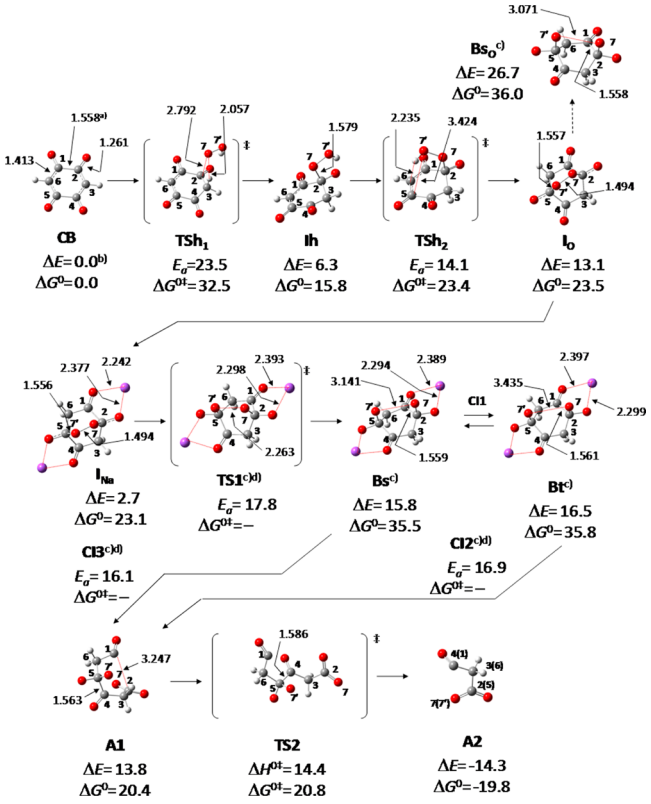

Figure 4. Proposed detailed mechanism for the degradation of DHBQ under moderately alkaline (pH 10) conditions, computed at the MP2/BS-II//DFT(B3LYP)/BS-I level of theory. Notes: (a) Bond lengths are given in Å. (b) Energy values are presented in kcal/mol. (c) Energies of **TS1**, $\mathbf{Bs}_O$, **Bs**, **Bt**, **CI2**, and **CI3** are calculated according to the DFT(UB3LYP)/BS-II method relative to the DFT(RB3LYP)/BS-II-calculated energy of $\mathbf{I}_{Na}$ because the MP2 method did not provide reliable energy data due to an instability of the Hartree–Fock wave functions for these species. (d) The structures of **TS1**, **CI2**, and **CI3** are approximated ones, and the potential energies do not include the zero-point energy; see Figures 5 and 8 and the pertinent discussion in the text.

conjugate base of $\mathbf{I}_{OH}$. Under the pH 10 conditions, DHBQ is completely converted into its dianionic conjugate base **CB** (Scheme 1) since the pK_{a1} and pK_{a2} of DHBQ are 2.95 and 4.87, respectively.[8] Although H_2O_2 is also a very weak acid, formation of deprotonated H_2O_2 such as HOO^- should not be predominant at pH 10 from its high pK_a of 11.7.[9] We thus investigated a reaction in which **CB** is attacked by H_2O_2 to form $\mathbf{I}_O$, using computations at the MP2//DFT(B3LYP) level of theory.

The detailed mechanism including the transition states is shown in Figure 4, and schematic description of the mechanism is shown in Scheme 3. The first step is a proton transfer from H_2O_2 to **CB** followed by nucleophilic attack of the resulting HOO^- to the C-2 carbonyl group, to form intermediate **Ih**. This reaction proceeds via transition state $\mathbf{TSh}_1$. In the second step, **Ih** is transformed to $\mathbf{I}_O$ through an intramolecular reaction via transition state $\mathbf{TSh}_2$. The mechanism of the formation of $\mathbf{I}_O$ from **Ih** is similar to that of the first step (**CB** to **Ih**): a proton transfer from the second hydrogen peroxide oxygen (O-7′) to C-6 and a subsequent nucleophilic attack of the anionic O-7′ at C-5 (see Figure 4). The rate-determining step in the formation of $\mathbf{I}_O$ is the first H_2O_2 attack, with the $\Delta^{\ddagger}G^{\circ}$ value (32.5 kcal/mol) of $\mathbf{TSh}_1$ being higher than that of $\mathbf{TSh}_2$ (23.4 kcal/mol). $\mathbf{I}_O$ was calculated to be 23.5 and 13.1 kcal/mol less stable than **CB** based on Gibbs energy and potential energy, respectively.[10]

The next step, also by analogy to the reaction in neutral medium, should be the O-7–O-7′ homolysis of $\mathbf{I}_O$. Hence, the singlet biradical $\mathbf{Bs}_O$, as the most plausible product, was considered at the DFT(UB3LYP) level (see Figure 4).[11] However, the obtained potential energy of $\mathbf{Bs}_O$ (26.7 kcal/mol) was so high that it far exceeded the experimental E_a value (see Figure 4 and Table 1). This led us to assume coordination of Na^+ to $\mathbf{I}_O$, with the electrostatic interaction between O^- and Na^+ stabilizing $\mathbf{I}_O$. As expected, the ΔE value of $\mathbf{I}_O$ was substantially decreased to 2.7 kcal/mol (coordination of two Na^+ ions; see $\mathbf{I}_{Na}$ in Figure 4). Because this coordination is entropically unfavored, the Gibbs energy of $\mathbf{I}_{Na}$ becomes comparable to that of $\mathbf{I}_O$, suggesting that $\mathbf{I}_O$ and $\mathbf{I}_{Na}$ are in equilibrium in water solution. We also calculated the corresponding singlet biradical **Bs** formed by O–O homolysis, **Bs** thus being the Na^+-coordinated $\mathbf{Bs}_O$. The potential energy of **Bs** (15.8 kcal/mol) is much lower than that of $\mathbf{Bs}_O$. From these lines of results, we focused our further investigation on the Na^+-coordinated species, such as $\mathbf{I}_{Na}$ and **Bs**, rather than on the anionic, noncoordinated ones. It should be also noted that our assumption of the Na^+ coordination is well supported by the above experimental facts: the addition of the sodium salts significantly increasing the reaction rate and the reaction under the moderately alkaline conditions being entropically unfavored (see previous section). The enhanced sodium cation concentration will shift the equilibrium between $\mathbf{I}_O$ and $\mathbf{I}_{Na}$ further to $\mathbf{I}_{Na}$, resulting in an enhanced homolysis rate of the O–O bond.

Since the geometry of **Bs** was optimized as a stable species at the DFT(UB3LYP) level, there must be a transition state that connects $\mathbf{I}_{Na}$ and **Bs**. The geometry optimization of such transition state, however, was neither successful with the restricted nor the unrestricted DFT(B3LYP) methods. Instead, the potential energy curve of the path from $\mathbf{I}_{Na}$ to **Bs** was investigated in regard to the dependence of the O-7–O-7′ bond length, this way approximating the structure of the transition state. As shown in Figure 5, the potential energy increases up to a O-7–O-7′ distance of 1.889 Å and then decreases again from a distance of 2.263 Å, indicating that the transition state is located between these O-7–O-7′distances. The failure to localize any transition state structure is due to the fact that exactly in this distance range the scission of the O–O bond occurs, which requires treatment by different computational methods for nonradical and radical species, i.e., RB3LYP and UB3LYP, making it impossible to run the geometry optimization constantly. We eventually decided to employ the geometry optimized at a O-7–O-7′ distance of 2.263 Å (**TS1** in Figures 4 and 5) for the determination of the activation energy,

dx.doi.org/10.1021/jo401486d | J. Org. Chem. 2013, 78, 11194–11203

Scheme 3. Schematic Description of the Detailed Mechanism for the Degradation of DHBQ under Moderately Alkaline (pH 10) Conditions

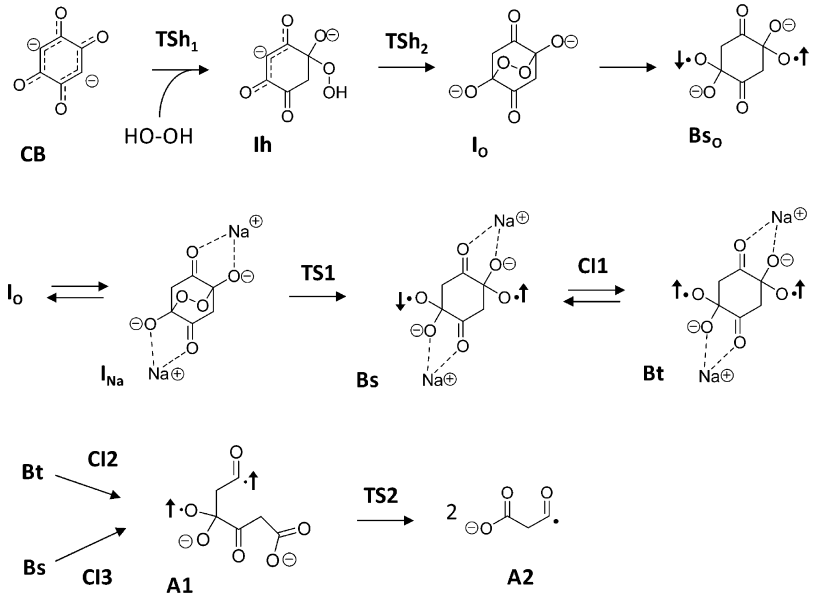

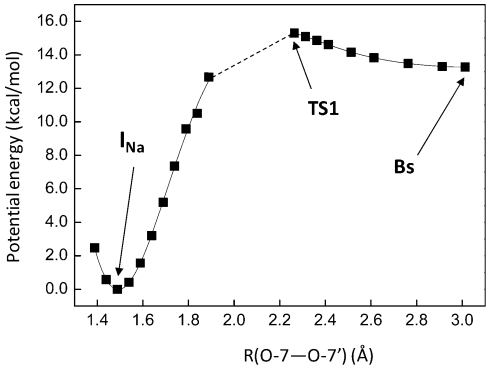

Figure 5. Potential energy curve regarding the O7—O7′ length from I_{Na} to **Bs**, computed at the DFT(UB3LYP)/BS-I level of theory. We obtained the potential energy curve by carrying out the geometry optimization with the O7—O7′ length set to the respective values.

as its structure is considered to be the closest to that of the actual transition state. As frequency calculation is meaningless in this case, the $\Delta^{\ddagger}G^{\circ}$ value was not determined; the obtained E_a value for **TS1** was 17.8 kcal/mol relative to **CB**.

We also optimized the structure of a triplet biradical **Bt**, the structure and energy of which were quite similar to those of **Bs**; see Figure 4 and Scheme 3. These results suggest that **Bs** and **Bt** are able to interconvert through a conical intersection **CI1** after O-7—O-7′ homolysis.

The detailed electronic structures of the biradical **Bs** and **Bt** were worth investigating in detail for a better understanding of the degradation mechanism. In this paragraph, we thus wish to discuss the electronic structure of **Bt** on the basis of its molecular orbitals calculated at the ROHF/BS-II level of theory. As shown in Figure 6A, the p-orbitals of O-7 and O-2 as well as those of O-7′ and O-5 interact with each other by σ-like antibonding and evenly contribute to the SOMOs (singly occupied molecular orbitals) of **Bt**; see Scheme 4A. The HOMO-5 and HOMO-6 of **Bt** involve the bonding counterparts of this interaction. The p-orbital of O-7 (the unpaired electron) and the p-orbital of O-2 (the lone-pair electrons) have similar orbital energies with strong σ-like interaction. This interaction destabilizes one electron and stabilizes two electrons, leading to overall stabilization of the biradical: $E_{SO} = 2\Delta E_{1O} - \Delta E_{2O} > 0$, see Scheme 4A. Since the biradical molecule is symmetric, the same interaction exists also between the unpaired electron of O-7′ and the lone pair electrons of O-5. The atomic charges and the spin densities of **Bt**, calculated at the DFT(UB3LYP)/BS-II level, showed that O-2, O-7, O-7′, and O-5 have almost the same atomic charges around −0.68 and spin densities around +0.55, indicating that the electrons are evenly delocalized between those atoms (Figure 7A). This result is consistent with the orbital interaction in Scheme 4A. The electronic structure of **Bs** was essentially the same as that of **Bt**; see Figure S5 in the Supporting Information for the important orbitals of **Bs**.

Then in the triplet state biradical **Bt** undergoes β-fragmentation to form an acyl radical anion **A1** (see Figure 4). Interestingly, this reaction needs to pass through a conical intersection **CI2**, which connects the most stable triplet state (T1) of **Bt** to the next stable triplet state (T2), see Figure 6A and B. To clarify the reason for the necessity of this conical intersection, we studied the electronic structure of **Bt** in the T2 state (T2-**Bt**). The important orbitals of T2-**Bt** show that one of the SOMOs (HOMO-1) contains the p-orbital of O-7 orthogonal to the SOMO of T1-**Bt**. In addition, the p-orbital of O-7 interacts with a p-orbital of C-2 in a π-like antibonding way with the bonding counterpart of this interaction in the HOMO-8. As shown in Scheme 5, T1-**Bt** cannot undergo the β-fragmentation because the p-orbital of C-2 cannot interact with the unpaired electron. In T2-**Bt**, on the other hand, the unpaired electron of O-7 does interact with the p-orbital of C-2, rendering β-fragmentation possible. This notion is also supported by the potential energy curves in Figure 8, where the T2 curve leads to **A1** while that of T1 monotonously increases. The energy of the T2 state of **Bt** is only 3.2 kcal/mol higher than that of the T1 state, calculated at the DFT-(UB3LYP)/BS-II level. Also, the T2 state becomes more stable than the T1 state when the C-1—C-2 bond is elongated by 0.05 Å from the equilibrium structure of T1-**Bt** (see **CI2** in the

dx.doi.org/10.1021/jo401486d | J. Org. Chem. 2013, 78, 11194—11203

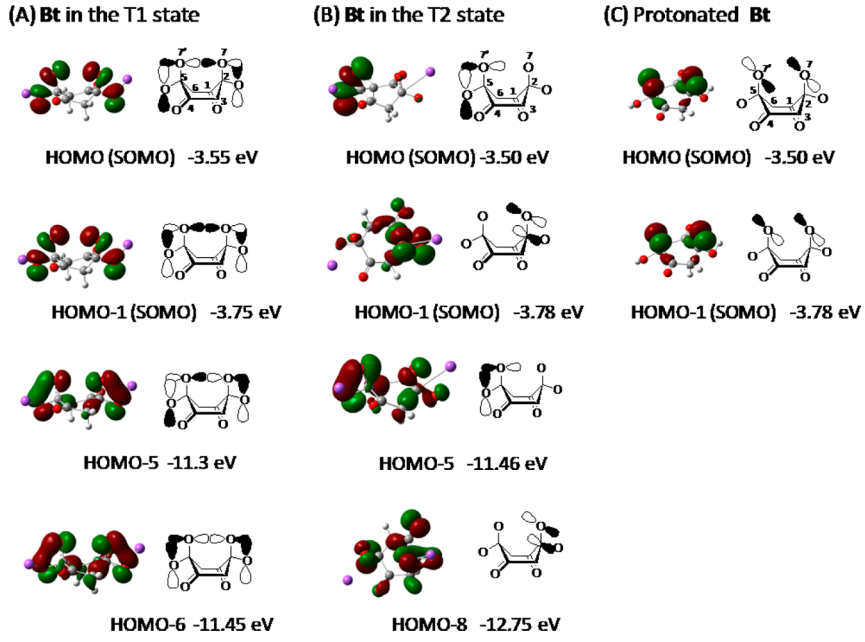

Figure 6. Important molecular orbitals of **Bt** in the T1 and T2 states and of the protonated **Bt** for comparison, calculated according to the ROHF/BS-I method.

Scheme 4. Difference in Orbital Interactions between Bt (A) and Protonated Bt (B)

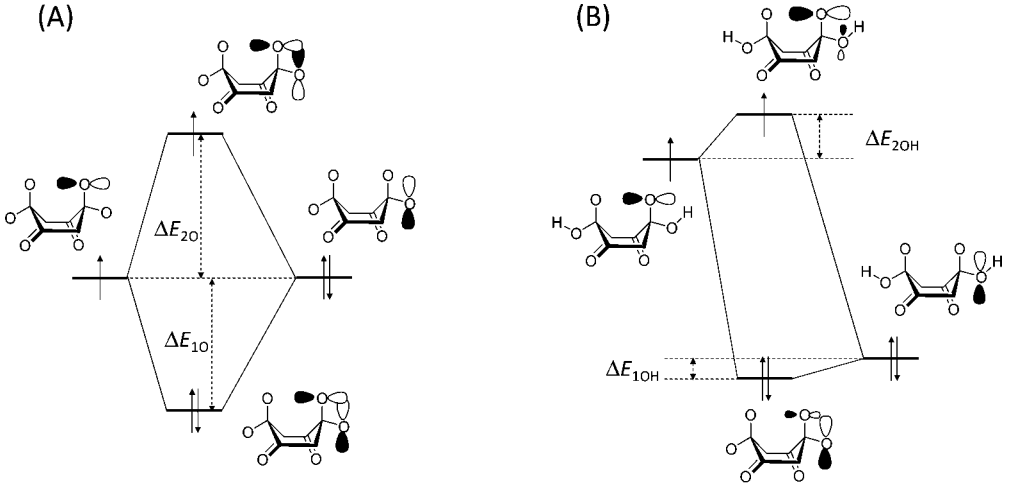

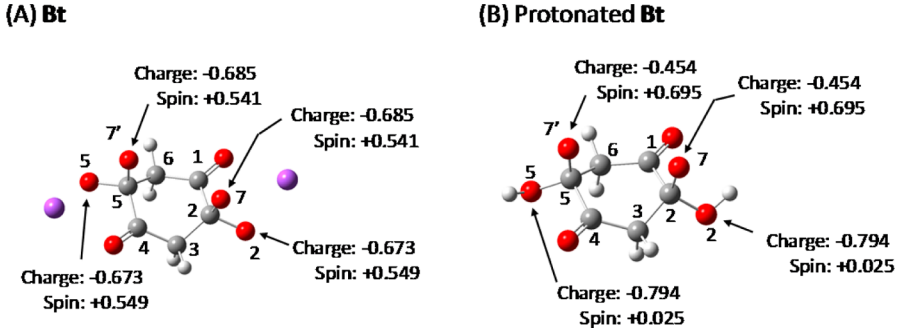

Figure 7. NBO atomic charges and Mulliken spin densities of important atoms of **Bt** and protonated **Bt** in the T1 state, calculated at the DFT(UB3LYP)/BS-II level of theory, where α spin is taken to be positive. The geometry of protonated **Bt** was obtained by geometry optimization, starting from that of **Bt**.

dx.doi.org/10.1021/jo401486d | J. Org. Chem. 2013, 78, 11194−11203

Scheme 5. Difference in Orbital Interactions between the T1 and T2 States of Bt

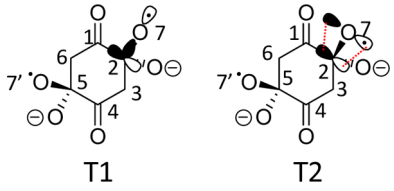

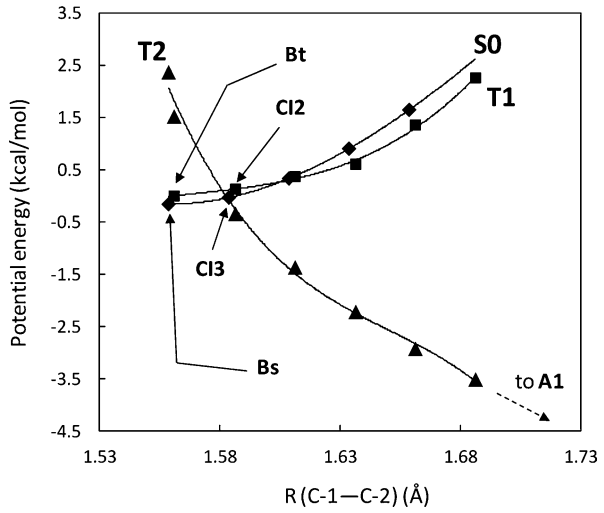

Figure 8. Potential energy curves of the S0 (◆), T1(■), and T2 (▲) states of the biradicals in regard to the C1−C2 distance, calculated according to the DFT(UB3LYP)/BS-I method. The potential energy curve was obtained by geometry optimization with the C-1−C-2 lengths fixed at the specified values.

potential energy curve in Figure 8). Although determination of the exact E_a value for this T1-to-T2 transition is not trivial, we estimated it to be 16.9 kcal/mol relative to **CB** (Figure 4) at the DFT(B3LYP)/BS-II level by assuming the geometry of **CI2** in Figure 8 as a reference for the real conical intersection structure. **Bs** in the S0 state can also change its spin state to the T2 state through another conical intersection **CI3** (see Figure 8). We estimated the E_a value for **CI3** to be 16.1 kcal/mol, assuming the geometry of **CI3** for the real conical intersection.

After the formation of **A1**, another type of β-fragmentation occurs to yield two molecules of a malonyl radical anion **A2** via **TS2** with a small activation energy of 14.4 kcal/mol (see Figure 4 and Scheme 3). **A2** readily produces malonic acid through further attack of H_2O_2, according to the literature.[12] The most plausible mechanism for the formation of malonic acid from **A2** involves several reaction steps, as shown in Scheme 6: H-abstraction by **A2** from H_2O_2 to form the corresponding aldehyde and an OOH radical, disproportionation of OOH radical to gaseous O_2 and H_2O_2, and further oxidation of the aldehyde into malonic acid. Though we did not investigate these reactions in detail, the above mechanism is supported by an experimental observation of gaseous oxygen formed during the degradation (see Figure S6 in Supporting Information).

The overall computed reaction pathway in Figure 4 and Scheme 3 accounts for the overall conversion of DHBQ into malonic acid in a plausible way agreeing with the experimental fact that malonic acid is formed from DHBQ in quantitative yield (see the previous section). The reaction energy of the whole degradation is considerably negative: −19.8 kcal/mol

Scheme 6. Suggested Mechanism of the Formation of Malonic Acid from Radical A2

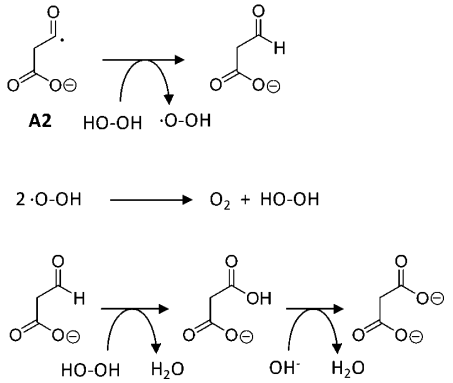

based on the Gibbs energy and −14.3 kcal/mol based on the potential energy. The rate-determining step in the overall process is the O-7−O-7′ homolysis of $\mathbf{I}_{Na}$ to form **Bs**, with **TS1** having the considerably high potential energy of 17.8 kcal/mol. When the entropy calculated for **Bs** was adapted to **TS1**, the $\Delta^{\ddagger}G^{\circ}$ value for **TS1** was estimated to be 36.8 kcal/mol, which was much higher than that in the $\mathbf{I}_O$ formation (32.5 kcal/mol, see above). The E_a value for **TS1** is in good agreement with the experimental E_a and $\Delta^{\ddagger}H^{\circ}$ values in Table 1, indicating that the proposed mechanism in Figure 4 was likely to be correct.

The formation of malonic acid could be theoretically explained also by ionic reactions as shown in Scheme 7.

Scheme 7. Hypothetic Ionic Degradation of the Intermediate Ih

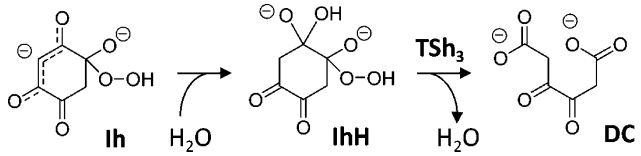

According to this hypothetic ionic mechanism, one of the keto groups of the intermediate **Ih** is first hydrolyzed to form **IhH**, followed by ionic β-fragmentation of **IhH** into dicarboxylic acid **DC** and water. The diketo group of **DC** reacts analogously to afford two molecules of malonic acid. To check whether this ionic mechanism is competitive, we simulated the reaction from **IhH** to **DC**. **IhH** was 34.3 kcal/mol less stable than the reactant **CB** based on Gibbs energy. We then optimized the transition state $\mathbf{TSh}_3$ connecting **IhH** to **DC**; see Figure S7 in Supporting Information for detailed geometry change in this reaction. The $\Delta^{\ddagger}G^{\circ}$ and E_a values of $\mathbf{TSh}_3$ were calculated to be 51.7 and 41.5 kcal/mol, respectively. Since these $\Delta^{\ddagger}G^{\circ}$ and E_a values for $\mathbf{TSh}_3$ were much larger than those of **TS1** (see above), it was evident that the ionic reaction via $\mathbf{TSh}_3$ was much less favorable than that via **TS1**. From these lines of computational results, we ruled out the hypothetical ionic mechanism.

Degradation of DHBQ under Moderately Alkaline (Buffered, pH 10) and Nonbuffered, Neutral Conditions: A Comparison. The mechanism for the degradation of DHBQ under pH 10 conditions is considerably different from that under the nonbuffered conditions.[5] In the upcoming section, we would like to address those differences and elaborate the reasons for them.

dx.doi.org/10.1021/jo401486d | J. Org. Chem. 2013, 78, 11194−11203

One important difference is the stability of the biradicals formed by the O−O bridge homolysis of the intermediates $\mathbf{I_O}$ (alkaline) and $\mathbf{I_{OH}}$ (neutral, nonbuffered). While **Bs** and **Bt** are stable species as discussed in the previous section (Figure 4 and Scheme 3), the conjugate acid of **Bs** and **Bt**, formed by the O−O bond homolysis of $\mathbf{I_{OH}}$ in the nonbuffered system (Scheme 1), is not a stable species, as reported in our previous study.[5] In other words, deprotonation of the two hydroxyl groups of $\mathbf{I_{OH}}$ stabilizes the biracial and renders it stable as intermediate species. In fact, the E_a value calculated for the degradation under the pH 10 conditions (17.8 kcal/mol, Figure 4) is much lower than that calculated for the degradation under the nonbuffered conditions (23.3 kcal/mol) reported in our previous study,[5] and so are the experimental E_a values (16.1 kcal/mol vs 20.4 kcal/mol, see Table 1). It was thus worth clarifying what changes in the electronic structure of **Bt** are caused by the protonation/deprotonation.

As described in the previous section, **Bt** is stabilized by the orbital interaction shown in Figure 6A and Scheme 4A. For comparison, Figure 6C shows the important molecular orbitals of the protonated **Bt**, also calculated at the ROHF/BS-I level of theory. Contrary to the SOMOs of **Bt**, the SOMOs of the protonated **Bt** are almost localized at p-orbitals of O-7 and O-7′; compare the orbitals in Figures 6A to those in 6C for that particular feature. The spin density of the protonated **Bt** is much higher at O-7 and O-7′ (+0.695) than at O-2 and O-5 (+0.025), while the negative charge is higher at O-2 and O-5 (−0.794) than at O-7 and O-7′ (−0.454). These results indicate that the delocalization of the spin and charge between O-7, O-7′, O-2, and O-5, which considerably stabilized **Bt** (Figure 6B), scarcely exist in the protonated **Bt**. The reason for this change is displayed in Scheme 4B: the orbital energies of the O-2 and the O-5 lone pairs are significantly lowered by protonation, and the energy difference between the O-7 and O-7′ single electrons and the O-2 and O-5 lone-pair electrons becomes significantly larger. The stabilizing interaction between these orbitals is thus substantially weakened: $E_{SOH} \ll E_{SO}$. The changes in the orbital interaction caused by the protonation of **Bt** will lead to a much higher potential energy of the protonated **Bt** compared to that of the original **Bt**, and this fact is very likely to be a major reason why **Bt** can exist as a stable species, but the conjugate acid (the protonated **Bt**) cannot.

Another important difference in the degradation reaction under the pH 10 and nonbuffered conditions is the product distribution: DHBQ produces malonic acid in quantitative yield in alkaline medium, while a maximum of 50% yield was obtained under neutral conditions.[5] This difference in the products is well explained from the difference in the spine state from which the β-fragmentation of the biradicals starts. In the T2 state of **Bt** (pH 10 conditions), the two unpaired electrons have the same spin so that they cannot form a covalent bond. Thus, β-fragmentation does not proceed further to form nonradical species after the formation of **A1**, and two molecules of a malonyl radical anion are formed (see a schematic description in Scheme 8). Under nonbuffered conditions, on the other hand, such a triplet state is only involved in a minor pathway, as previously reported,[5] while the major degradation path starts from the singlet (S0) state in which the unpaired electrons can readily form a covalent bond after the β-fragmentation due to their different spin. Hence, ketene and oxaloacetic acid **OA** are produced as nonradical products. Since only **OA** is a precursor of malonic acid, its yield comes down to 50% under nonbuffered conditions (cf. Scheme 2).

Scheme 8. Mechanism of the β-Fragmentation from Bt to A2 via A1

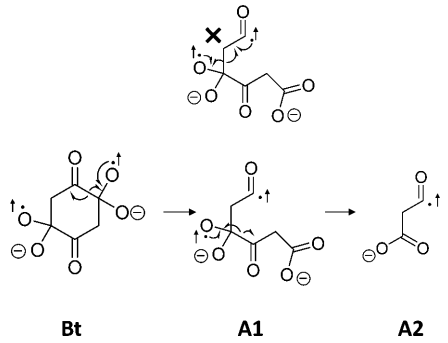

CONCLUSIONS

We have investigated the degradation of DHBQ by H_2O_2 in alkaline medium (pH 10, buffer). Kinetic and product analysis showed DHBQ to be degraded into malonic acid in quantitative yield with an E_a value of 16.1 kcal/mol. The mechanism of the degradation under the pH 10 conditions was thus significantly different from that under the nonbuffered conditions. This clearly disqualifies the conventional assumption in pulp bleaching with H_2O_2 (P-stage) that a change in pH influences only the reaction rate for chromophore removal, but not the actual mechanism.

The clarified mechanism under alkaline conditions of about pH 10 is as follows: (1) the reaction of DHBQ with H_2O_2 results in the formation of an addition product, intermediate $\mathbf{I_O}$. DHBQ is reacting in the form of its dianion **CB**, so that also $\mathbf{I_O}$ is a dianion. (2) $\mathbf{I_O}$ suffers homolytic O−O bond cleavage to form biradical **Bs** in the S0 state and **Bt** in the T1 state. This step is much facilitated by addition of Na^+. (3) **Bs** and **Bt** change the electronic structure to the T2 state through the conical intersections and then undergo β-fragmentation to form the acyl radical anion **A1**. (4) **A1** is further degraded into the malonyl radical anion **A2**, which finally is neatly converted to malonic acid by the attack of excess H_2O_2.

The beneficial effect of Na^+, which is significantly stabilizing $\mathbf{I_O}$ and in this way increasing the homolysis rate, is supported both by the experimental data and the theoretical calculation. The addition of salts, such as sodium sulfate that is a byproduct in many pulp production units anyway, during the P-stage would be an interesting conclusion to be tested in real-world bleaching of cellulosic pulps. The kinetic analyses and the computation indicated DHBQ to be degraded more easily under the pH 10 conditions than under the neutral conditions. In a P-stage, alkaline media are used anyway in order to minimize damage to the carbohydrate that significantly increases with pH decreasing. The use of an alkaline pH would now get additional support as it is needed not only from the viewpoint of carbohydrate preservation but also with regard to a faster degradation of DHBQ-based chromophores.

Another conclusion is that a very high pH (14 and above) is negative from the viewpoint of DHBQ degradation. The first step of the degradation sequence, attack of neutral H_2O_2 at the dianionic form of DHBQ, would be strongly impeded if H_2O_2 is deprotonated, due to repulsion between the two negatively charged reaction partners. Thus, a very high pH is not beneficial with regard to DHBQ discoloration; a pH between 10 and 12 is most appropriate in this regard and in addition saves alkali, which is one of the main cost factors in P-stages.

dx.doi.org/10.1021/jo401486d | J. Org. Chem. 2013, 78, 11194−11203

The studied mechanisms of DHBQ degradation by hydrogen peroxide suggest that both reaction rate and reaction mechanism (and thus product distribution) are controlled by the pH since the underlying (de)protonation processes change the stability and the reactivity of the biradical formed by the O−O bond homolysis of the respective intermediates. We hope that the insights will be helpful with regard to improving the efficiency of pulp bleaching processes.

EXPERIMENTAL AND COMPUTATIONAL DETAILS

Experimental Section. All chemicals were purchased from commercial providers. They were of highest purity available (p.a. grade) and were used without further purification. Proton nuclear magnetic resonance (^{1}H NMR) spectra were recorded at 400.13 MHz proton resonance frequency.

The degradation reaction was started by adding a 30% aqueous solution of hydrogen peroxide (2.2 mL, 19.6 mM of hydrogen peroxide) to 20 mL of an pH 10 buffer solution (NaOH-borax) of DHBQ (10.7 mg, 0.0763 mM) in a 50 mL round-bottom flask. The buffer solution of DHBQ contained 4.0 mg of 1,3,5-tricarboxylbenzene as internal standard. The solution of DHBQ was preheated at temperatures between 278.15 and 323.15 K before addition of the hydrogen peroxide solution. After the reaction started, sampling of the reaction mixture was done by adding 2.0 mL of the reaction solution separately into 10.0 mL of a 0.005 M HCl solution and 10.0 mL of deionized water, to obtain two types of the sample: sample **A** is prepared from the 0.005 M HCl solution, and sample **B** from the pure water. These samples were then immediately cooled to 0 °C in an ice bath and frozen at 193.15 K. After freeze-drying of the samples at this temperature, sample **A** was analyzed by ^{1}H NMR in DMSO-d_6 to quantify the amount of nonreacted DHBQ. Sample **B** was monitored with ^{1}H NMR in D_2O. Since sample **B** is not neutralized with HCl during its preparation, all acids produced from DHBQ exist as their corresponding sodium salts, which are not removed in the freeze-drying process.

The degradation of DHBQ was also carried out in the presence of 1.63 g (11.4 mM) of sodium sulfate. In this case, sodium sulfate was added into the buffer solution of DHBQ in advance, and the degradation was started in the same manner as described above. Sampling was carried out according to the procedure described above for sample **A**. The freeze-dried mixture was extracted with dimethyl ether, and the soluble part was subject to ^{1}H NMR analysis in DMSO-d_6 after removal of the solvent *in vacuo*.

Computations. We employed the GAUSSIAN 09 program packages for the calculations.[13] The geometry optimization in water was carried out by the DFT method with the B3LYP functional[14] and the PCM method. The 6-31G(d) basis sets were employed for H, C, O, Na where a diffuse function was added to each of C and O and a p-polarization function was added to H. We name these basis sets as BS-I. For single point calculations, we employed MP2 or DFT(UB3LYP) method, the latter was used only for the calculations of **I**, **Bs**, and **Bt**. The DFT(UB3LYP) functional is adequate to evaluate the property of O−O bonds as we reported before,[5] while the MP2 method did not work due to the instability of the wave function that arises from the homolysis of the O−O bond. In the single point calculations, cc-pVDZ basis stets were employed for H and Na, and aug-cc-pVDZ basis sets were employed for C and O. These basis sets are named as BS-II.

In all calculations, the solvation energy was evaluated with the PCM method. For the determination of the cavity size in the PCM calculation, the UFF parameters were used along with the united atom topological model optimized for the HF/6-31G(d) level of theory for geometry optimization and energy evaluation, respectively. It was ascertained that each equilibrium geometry exhibited no imaginary frequency and each transition state exhibited one imaginary frequency. Enthalpy, entropy, and Gibbs energy changes were evaluated at 298.15 K. Zero-point energy, thermal energy, and entropy change were evaluated with the DFT(B3LYP) method. The translational entropy in water was evaluated according to the literature method.[15]

ASSOCIATED CONTENT

Supporting Information

Complete ref 13. ^{13}C NMR and ^{11}B NMR spectra of the degradation reaction at 298.15 K and 240 s, sample **A** in DMSO-d_6. Total-ion chromatogram in GC−MS analysis (after trimethylsilylation) of degradation reaction at 298.15 K and 240 s, sample **A**. Relationships between ln[DHBQ] and t in the degradation of DHBQ under the presence of sodium sulfate and sodium chloride. Arrhenius plot in the degradation of DHBQ under the presence of sodium sulfate. Important orbitals of **Bs**. Picture of the reaction solution under the pH 10 conditions. Geometry changes and energy profile in the ionic degradation of DHBQ. Cartesian coordinates of the optimized geometries. This material is available free of charge via the Internet at http://pubs.acs.org.

AUTHOR INFORMATION

Corresponding Author

*E-mail: thomas.resenau@boku.ac.at.

Notes

The authors declare no competing financial interest.

ACKNOWLEDGMENTS

We performed quantum chemical calculations with the workstation in the Sakaki group, Fukui institute for fundamental chemistry at Kyoto University, Japan and are thankful for the access. The financial support of the Austrian Christian Doppler Research Society (CDG) through the CD-lab "Advanced cellulose chemistry and analytics" and of the Austrian Research Promotion Agency (FFG, project 829443) is gratefully acknowledged.

REFERENCES

(1) (a) Rosenau, T.; Potthast, A.; Milacher, W.; Hofinger, A.; Kosma, P. *Polymer* **2004**, *45*, 6437. (b) Rosenau, T.; Potthast, A.; Milacher, W.; Adorjan, I.; Hofinger, A.; Kosma, P. *Cellulose* **2005**, *12*, 197. (c) Rosenau, T.; Potthast, A.; Kosma, P.; Suess, U.; Nimmerfroh, N. *Holzforschung* **2007**, *61*, 656. (d) Krainz, K.; Potthast, A.; Suess, U.; Dietz, T.; Nimmerfroh, N.; Rosenau, T. *Holzforschung* **2009**, *63*, 647. (e) Rosenau, T.; Potthast, A.; Krainz, K.; Yoneda, Y.; Dietz, T.; Shields, Z. P.; French, A. D. *Cellulose* **2011**, *18*, 1623.

(2) Hosoya, T.; French, A. D.; Rosenau, T. *Mini-Rev. Org. Chem.* **2013**, *10*, 309.

(3) (a) Brassard, P.; L'Ecuyer, P. *Can. J. Chem.* **1958**, *36*, 1346. (b) Nicolaides, D. N.; Gautam, D. R.; Litinas, K. E.; Papamehael, T. *J. Chem. Soc., Perkin Trans. 1* **2002**, 1455. (c) Lang, M.; Muhlbauer, A.; Jagers, E.; Steglich, W. *Eur. J. Org. Chem.* **2008**, *20*, 3544. (d) Shaabani, A.; Ghadari, R.; Sarvary, A.; Rezayan, A. *J. Org. Chem.* **2009**, *74*, 4372. (e) Shaabani, A.; Ghadari, R.; Ghasemi, S.; Pedarpour, M.; Rezayan, A.; Sarvary, A.; Ng, S. W. *J. Comb.* **2009**, *11*, 956. (f) Misiolek, A.; Ichimura, A. S.; Gentner, R. A.; Huang, R. H.; McCaffrey, V. P.; Jackson, J. E. *Inorg. Chem.* **2009**, *48*, 9005. (g) Jimenez-Alonso, S.; Estevez-Braun, A.; Ravelo, A. G.; Zarate, R.; Lopez, M. *Tetrahedron* **2007**, *63*, 3066. (h) Jimenez-Alonso, S.; Perez-Lomas, A. L.; Estevez-Braun, A.; Martinez, F. M.; Orellana, H. C.; Ravelo, A. G.; Gamarro, F.; Castanys, S.; Lopez, M. *J. Med. Chem.* **2008**, *51*, 7132. (i) Koulouri, S.; Malamidou-Xenikaki, E.; Spyroudis, S. *Tetrahedron* **2005**, *61*, 10894.

(4) (a) Manthey, M. K.; Pyne, S. G.; Truscott, R. J. W. *Aust. J. Chem.* **1989**, *42*, 365. (b) Ikeda, M.; Kitahara, K.; Nishi, H. *J. Heterocycl. Chem.* **1992**, *29*, 289. (c) Zhang, D.; Jin, G. X. *Organometallics* **2003**, *22*, 2851. (d) Gellerman, G.; Rudi, A.; Kashman, Y. *Tetrahedron* **1994**, *50*, 12959. (e) Reuben, G.; Shonle, H. A. *J. Am. Chem. Soc.* **1946**, *68*, 2246. (f) Placin, F.; Clavier, G.; Najera, F.; Desvergne, J. P.; Pozzo, J. L. *Polycyclic Aromat. Compd.* **2000**, *19*, 107. (g) Lehaire, M. L.;

Scopelliti, R.; Herdeis, L.; Polborn, K.; Mayer, P.; Severin, K. *Inorg. Chem.* **2004**, *43*, 1609. (h) Seillan, C.; Brisset, H.; Siri, O. *Org. Lett.* **2008**, *10*, 4013. (i) Tang, Q.; Liu, J.; Chan, H. S.; Miao, Q. *Chem.—Eur. J.* **2009**, *15*, 3965. (j) Lee, D. C.; Cao, B.; Jang, K.; Forster, P. M. *J. Mater. Chem.* **2010**, *20*, 867. (k) Tang, Q.; Liang, Z.; Liu, J.; Xu, J.; Miao, Q. *Chem. Commun.* **2010**, *46*, 2977. (l) Di, C.; Li, J.; Yu, G.; Xiao, Y.; Guo, Y.; Liu, Y.; Qian, X.; Zhu, D. *Org. Lett.* **2008**, *10*, 3025.

(5) Hosoya, T.; Rosenau, T. *J. Org. Chem.* **2013**, *78*, 3176.

(6) Since the borate ester is water-sensitive and alkali-sensitive, the ester is not formed during the degradation and thus has no effect in the kinetic analysis.

(7) The degradation of DHBQ is much faster than that of malonic acid under the employed conditions. Hence, malonic acid was quantitatively produced from DHBQ.

(8) Mostafa, S. I. *Trans. Met. Chem.* **1999**, *24*, 306.

(9) Lee, H.; Park, A. H.; Oloman, C. *TAPPI J.* **2000**, *83*, 94.

(10) The ΔG° value is much higher than the E_a value due to decrease in entropy by the covalent bond formation between H_2O_2 and **CB**.

(11) The DFT(UB3LYP) calculations for $\mathbf{Bs}_O$ and **Bs** resulted in a considerable degree of spin contamination, but we have described that the DFT(UB3LYP) functional can reproduce a correct energy profile in the O−O bond cleavage of H_2O_2 (see ref 5).

(12) (a) Dagaut, P.; Wallington, T. J.; Kurylo, M. J. *J. Phy. Chem.* **1988**, *92*, 3836. (b) Vaghjiani, G. L.; Ravishankara, A. R. *J. Phys. Chem.* **1989**, *93*, 1948. (c) Lightfoot, P. D.; Veyret, B.; Lesclaux, R. *J. Phy. Chem.* **1990**, *94*, 708. (d) Lightfoot, P. D.; Lesclaux, R.; Veyret, B. *J. Phy. Chem.* **1990**, *94*, 700. (e) Wallington, T. J.; Dagaut, P.; Kurylo, M. J. *Chem. Rev.* **1992**, *92*, 667.

(13) Frisch, M. J., et al. *Gaussian 09, Revision A.1*; Gaussian, Inc.: Wallingford, CT, 2009. See Supporting Information for the complete description.

(14) (a) Becke, A. D. *Phys. Rev. A* **1988**, *38*, 3098. (b) Becke, A. D. *J. Chem. Phys.* **1983**, *98*, 5648.

(15) Mammen, M.; Shakhnovich, E. I.; Deutch, J. M.; Whitesides, G. M. *J. Org. Chem.* **1998**, *63*, 3821.